Identifying Oscillatory Hyperconnectivity and Hypoconnectivity Networks in Major Depression Using Coupled Tensor Decomposition

Wenya Liu, Xiulin Wang, *Student Member, IEEE*, Jing Xu, Yi Chang, Timo Hämäläinen, *Senior Member, IEEE*, and Fengyu Cong, *Senior Member, IEEE*

***Abstract*— Previous researches demonstrate that major depression disorder (MDD) is associated with widespread network dysconnectivity, and the dynamics of functional connectivity networks are important to delineate the neural mechanisms of MDD. Neural oscillations exert a key role in coordinating the activity of remote brain regions, and various assemblies of oscillations can modulate different networks to support different cognitive tasks. Studies have demonstrated that the dysconnectivity of electroencephalography (EEG) oscillatory networks is related with MDD. In this study, we investigated the oscillatory hyperconnectivity and hypoconnectivity networks in MDD under a naturalistic and continuous stimuli condition of music listening. With the assumption that the healthy group and the MDD group share similar brain topology from the same stimuli and also retain individual brain topology for group differences, we applied the coupled nonnegative tensor decomposition algorithm on two adjacency tensors with the dimension of time × frequency × connectivity × subject, and imposed double-coupled constraints on spatial and spectral modes. The music-induced oscillatory networks were identified by a correlation analysis approach based on the permutation test between extracted temporal factors and musical features. We obtained three hyperconnectivity networks from the individual features of MDD and three hypoconnectivity networks from common features. The results demonstrated that the dysfunction of oscillatory networks could affect the involvement in music perception for MDD patients. Those oscillatory dysconnectivity networks may provide promising references to reveal the pathoconnectomics of MDD and potential biomarkers for the diagnosis of MDD.**

***Index Terms*— Dynamic functional connectivity, coupled tensor decomposition, major depression disorder, naturalistic music stimuli, oscillatory networks.**

Manuscript received January 11, 2021; revised May 19, 2021 and August 5, 2021; accepted September 7, 2021. Date of publication September 9, 2021; date of current version September 17, 2021. This work was supported in part by the National Natural Science Foundation of China under Grant 91748105, in part by the National Foundation in China under Grant JCKY2019110B009 and Grant 2020-JCJQ-JJ-252, in part by the Fundamental Research Funds for the Central Universities in Dalian University of Technology, China, under Grant DUT2019 and Grant DUT20LAB303, and in part by the Scholarships from China Scholarship Council under Grant 201706060263 and Grant 201706060262. *(Corresponding author: Fengyu Cong.)*

This work involved human subjects or animals in its research. Approval of all ethical and experimental procedures and protocols was granted by the First Affiliated Hospital of Dalian Medical University.

Wenya Liu is with the Faculty of Electronic Information and Electrical Engineering, School of Biomedical Engineering, Dalian University of Technology, Dalian 116024, China, and also with the Faculty of Information Technology, University of Jyväskylä, 40014 Jyväskylä, Finland (e-mail: wenyaliu0912@foxmail.com).

Xiulin Wang is with the Department of Radiology, Affiliated Zhongshan Hospital of Dalian University, Dalian 116001, China, and also with the Faculty of Electronic Information and Electrical Engineering, School of Biomedical Engineering, Dalian University of Technology, Dalian 116024, China (e-mail: xiulin.wang@foxmail.com).

Jing Xu and Yi Chang are with the Department of Neurology and Psychiatry, First Affiliated Hospital, Dalian Medical University, Dalian 116011, China (e-mail: xujing.doc@aliyun.com; changee99@gmail.com).

Timo Hämäläinen is with the Faculty of Information Technology, University of Jyväskylä, 40014 Jyväskylä, Finland (e-mail: timo.t.hamalainen@jyu.fi).

Fengyu Cong is with the Faculty of Electronic Information and Electrical Engineering, School of Biomedical Engineering, Dalian University of Technology, Dalian 116024, China, also with the Faculty of Information Technology, University of Jyväskylä, 40014 Jyväskylä, Finland, also with the Faculty of Electronic Information and Electrical Engineering, School of Artificial Intelligence, Dalian University of Technology, Dalian 116024, China, and also with the Key Laboratory of Integrated Circuit and Biomedical Electronic System, Dalian University of Technology, Dalian, Liaoning 116024, China (e-mail: cong@dlut.edu.cn).

Digital Object Identifier 10.1109/TNSRE.2021.3111564

I. Introduction

MAJOR depression disorder (MDD) is a globally common psychiatric disorder characterized by deficits of affective and cognitive functions [1]–[3]. It is almost a consensus to researchers that MDD is accompanied by abnormal functional connectivity (FC) between some brain regions, like cortical regions in the default mode network (DMN), rather than the aberrant response of individual brain regions [3]–[6]. Music therapy is associated with improvements in mood, which has made it an attractive tool for MDD treatment [7]. Previous studies have suggested that the oscillatory asymmetry and dysconnectivity could be the potential biomarkers of MDD during music perception [8]–[10].

An increasing amount of researches have demonstrated that FC presents the potential of temporal variability across different time-scales (from milliseconds to minutes) to support continuous cognitive tasks. This is termed as dynamic functional connectivity (dFC), and it represents the processes by which networks and subnetworks coalesce and dissolve over time, or cross-talk between networks [11]–[13]. Recently, researches have reported abnormal dFC of specific brain regions and

neural networks in MDD using resting-state functional Magnetic Resonance Imaging (RS-fMRI) [3], [5], [13], [14]. For example, Demirtas *et al.* found a decreased variability of FC in the connections between the DMN and the frontoparietal network [5]. Kaiser *et al.* showed that MDD patients presented decreased dFC between medial prefrontal cortical (MPFC) regions and regions of parahippocampal gyrus within the DMN, but increased dFC between MPFC regions and regions of insula. They showed that MDD was related to abnormal patterns of fluctuating communication among brain systems involved in regulating attention and self-referential thinking [13]. The decreased dFC variability was reported between anterior DMN and right central executive network (CEN) in MDD, which indicated a decreased information processing and communication ability [14]. Existing researches about dFC in MDD mostly focus on resting-state conditions. However, little is known about the abnormalities of dFC during music listening conditions.

Benefiting from the high temporal resolution, electroencephalography (EEG) can record electrical brain activity dynamics at a millisecond scale with rich frequency contents. The oscillation acts as a bridge to connect different brain regions with resonant communication, which can regulate changes of neuronal networks and cause qualitative transitions between modes of information processing [15]–[17]. Impaired coordination of brain activity associated with abnormal electrophysiological oscillations contributes to the generation of psychaitric disorders [18]. Numerous studies have investigated EEG oscillatory FC of MDD in resting-state, and dysconnectivity networks are mostly notable in theta, alpha and beta oscillations [16], [19], [20]. However, most previous studies filter EEG signals into a range of frequency bands (e.g., 8-13 Hz for the alpha band), and ignore the exhaustive spectral dynamics in FC [19], [20]. Music perception is a complex cognitive task, which is characterized with dynamics of frequency-specific brain networks for musical features processing [21]–[25]. To the best of our knowledge, the oscillatory dFC in MDD during music perception has not been well investigated yet.

Considering the temporal dynamics and spectral modulations of spatial couplings (e.g., functional connectivity) for multiple participants in a cognitive task, a multi-way dataset structure is naturally formed. This multi-dimensional nature points to the adoption of tensor decomposition models instead of matrix decomposition models, which normally fold some dimensions and ignore the hidden interactions across different modes [24], [26]–[29]. Canonical Polyadic (CP) decomposition is derived in terms of the sum of multiple rank-one tensors, and each rank-one tensor represents the covariation of the corresponding components from each mode [30], [31]. The CP decomposition is well implemented into the extraction of multi-mode EEG features from the multiway dataset (e.g., channel $\times$ frequency $\times$ time $\times$ subject) [31]–[34]. Recently, Zhu *et al.* applied CP decomposition to explore the task-related dFC characterized by spatio-temporal-spectral modes of covariation from the adjacency tensor (connectivity $\times$ time-subject $\times$ frequency) [23], [35]. However, those applications only focus on the decomposition of one single tensor, which are based on the assumption that the underlying spatio-spectral features are consistent among subjects or groups [25], [29]. Coupled tensor decomposition (CTD), the extension of tensor decomposition to multiple block tensors, enables the simultaneous extraction of common features shared among tensors and individual features specified for each tensor. For biomedical data, the coupled matrix, matrix-tensor or tensor decomposition (also known as linked component analysis) are mostly used for data fusion [36]–[38]. However, to the best of our knowledge, no studies have used CTD to investigate the pathologic networks of MDD or other psychiatric disorders.

In our study, we applied a low-rank double-coupled nonnegative tensor decomposition (DC-NTD) model to explore the temporal and spectral dynamics of spatial couplings in MDD during music listening. The proposed analysis pipeline is totally data-driven. We analyzed the whole-brain FC to avoid prior knowledge about regions of interest, and we investigated the exhaustive assemblies of oscillations to avoid the selection of the frequency range. Figure 1 shows the diagram of the analysis pipeline of this study.

In this paper, scalars, vectors, matrices and tensors are denoted by lowercase, boldface lowercase, boldface uppercase and boldface script letters, respectively, e.g., x, $\boldsymbol{x}$, $\boldsymbol{X}$, $\boldsymbol{\mathcal{X}}$. Indices range from 1 to their capital version, e.g., $i = 1, \cdots, I$.

II. Materials and Methods

A. Simulated Data

To validate the feasibility of the proposed method, we firstly applied it on the simulated data. Two tensors with the size of 500 $\times$ 59 $\times$ 2278, representing time $\times$ frequency $\times$ connectivity, were created as follows:

$$\begin{aligned}\boldsymbol{\mathcal{X}}_1 &= \tilde{\boldsymbol{\mathcal{X}}}_1 + \boldsymbol{\mathcal{N}}_1 \\ &= t_1 \circ f_1 \circ c_1 + t_2 \circ f_2 \circ c_2 + t_3 \circ f_3 \circ c_3 + \boldsymbol{\mathcal{N}}_1, \quad (1)\\ \boldsymbol{\mathcal{X}}_2 &= \tilde{\boldsymbol{\mathcal{X}}}_2 + \boldsymbol{\mathcal{N}}_2 \\ &= t_4 \circ f_1 \circ c_1 + t_5 \circ f_2 \circ c_2 + t_6 \circ f_4 \circ c_4 + \boldsymbol{\mathcal{N}}_2, \quad (2)\end{aligned}$$

where $\tilde{\boldsymbol{\mathcal{X}}}_m, m = 1, 2$ represented the ground truth networks, and $\boldsymbol{\mathcal{N}}_n, n = 1, 2$ were the nonnegative noise created by the absolute values of white noise with the size of 500 $\times$ 59 $\times$ 2278. In the time domain, each temporal component $t_i, i = 1, 2, \cdots, 6$ was simulated by the absolute value of white noise to ensure the nonnegativity of the synthetic tensor $\boldsymbol{\mathcal{X}}$, and no coupled temporal component existed between two tensors. In the frequency domain, four spectral components $f_j, j = 1, 2, \cdots, 4$ were constructed by Hanning windows and white noise with bandwidth centered at 5 Hz, 10 Hz, 15 Hz and 20 Hz, and two spectral components were set to be coupled between two tensors. In the adjacency domain, four adjacency components $c_k, k = 1, 2, \cdots, 4$, representing auditory network (AUD), visual network (VIS), salience network (SAN), and dorsal attentional network (DAN), were constructed with the Desikan-Killiany anatomical atlas according to Kabbara's work [39], and two adjacency components were coupled between two tensors. The synthetic data were shown in Figure 2(a).

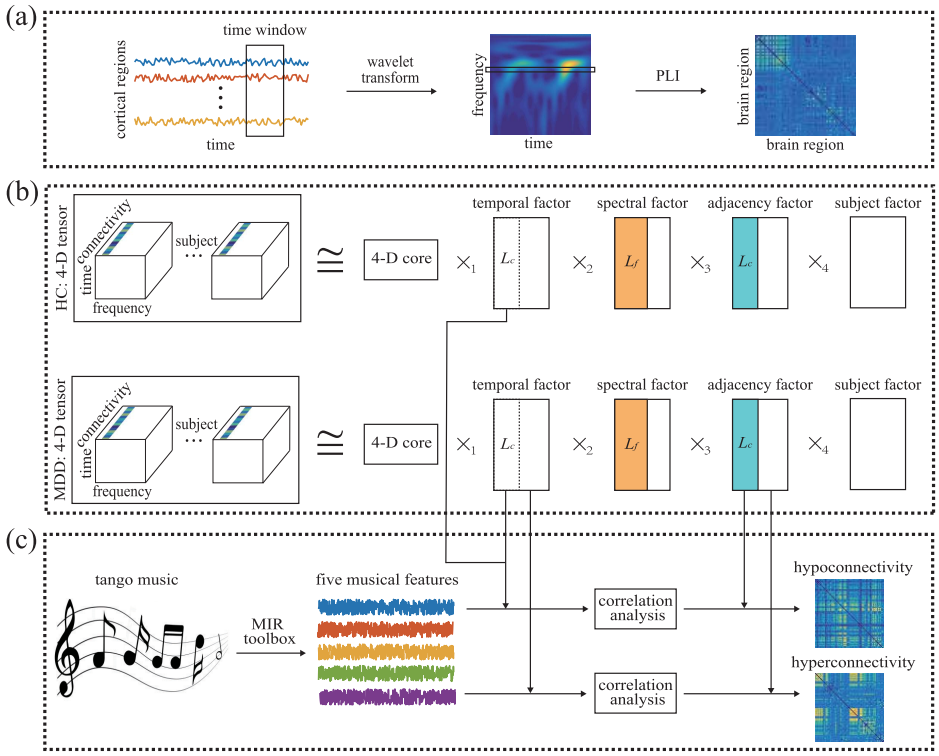

Fig. 1. Diagram of the analysis pipeline. (a) Adjcency matrix construction in each time window and each frequency bin. After source reconstruction, the cortical signals were segmented by overlapping time windows, and wavelet transform was applied for each time course within each time window. Phase lag index was used to obtain the adjacency matrix for each time window and each frequency bin. (b) Adjacency tensor construction and decomposition. A 4-D adjacency tensor was constructed for each group with the dimension of time × frequency × connectivity × subject, and coupled tensor decomposition was implemented with coupled constraints in spectral and adjacency modes. The 4-D core tensor is superdiagonal with values of 1. (c) The identification of hyperconnectivity and hypoconnectivity networks by music modulation. Five musical features were extracted with MIR toolbox from tango music, and correlation analysis was conducted between musical features and decomposed temporal factors to identify music-induced brain networks. Hyperconnectivity and hypoconnectivity networks were summarized from the results of music modulation.

B. EEG Data Description

1) Participants: Twenty MDD patients and nineteen healthy controls (HC) participated in this experiment. All the patients were from the First Affiliated Hospital of Dalian Medical University in China. This study has been approved by the ethics committee of the hospital, and all participants signed the informed consent before their enrollment. None of the participants has reported hearing loss and formal training in music. All the MDD patients were primarily diagnosed by a clinical expert and tested according to Hamilton Rating Scale for Depression (HRSD), Hamilton Anxiety Rating Scale (HAMA) and Mini-Mental State Examination (MMSE). The means and standard deviations (SD) of age, education, clinical measures, duration of illness and gender for both groups were listed in Table I.

2) EEG Data: During the experiment, participants were told to sit comfortably in the chair and listen to a piece of music. A 512-second musical piece of modern tango *Adios Nonino* by Astor Piazzolla was used as the stimulus due to its rich musical structure and high range of variation in musical features such as dynamics, timbre, tonality and rhythm [21], [40]. The EEG data were recorded by the Neuroscan Quik-cap device with 64 electrodes arranged according to the international 10-20 system at the sampling frequency of 1000 Hz. The electrodes placed at the left and right earlobes were used as the references.

TABLE I
MEANS AND STANDARD DEVIATIONS OF AGE, EDUCATION, CLINICAL MEASURES, DURATION OF ILLNESS AND GENDER FOR THE HC GROUP AND THE MDD GROUP

	HC group		MDD group		p-value
	Mean	SD	Mean	SD	
Age	38.4	11.8 (24-65)	42.9	11.0(23-58)	>0.05*
Education	13.6	3.8(6-20)	12.8	3.4(6-16)	>0.05*
HRSD	2.4	1.3(0-4)	23.3	3.6(16-28)	<0.01*
HAMA	2.4	1.3(0-5)	19.2	3.0(15-25)	<0.01*
MMSE	28.2	0.9(27-30)	28.1	1.1(26-30)	>0.05*
Duration	0	0	12.8	8.5(2-36)	-
Gender	14 females, 5 males		14 females, 6 males		>0.05**

Abbreviations: HC, healthy controls; MDD, major depression disorder; SD, standard deviations; HRSD, Hamilton Rating Scale for Depression; HAMA, Hamilton Anxiety Rating Scale; MMSE, Mini-Mental State Examination. The measure unit of duration is month, and the measure unit of age and education is year. *The p-value is calculated by t-test. **The p-value is calculated by chi-squared test.

The data were visually checked to remove obvious artifacts from head movement and down-sampled to $fs = 256$ Hz for further processing. Then 50 Hz notch filter and high-pass and low-pass filters with 1 Hz and 30 Hz cutoff were applied. We interpolated the bad intervals of one channel by

the mean values of their spherical adjacent channels. Eye movements artifacts were rejected by independent component analysis (ICA).

3) Musical Features: In this study, two tonal and three rhythmic features were extracted by a frame-by-frame analysis approach using MIR toolbox [41]. The duration of each frame was 3 seconds, and the overlap between two adjacency frames was 2 seconds. Therefore, we got 510 samples for the time courses of each musical feature at a sampling frequency of 1 Hz. In this study, we only used the first $T = 500$ samples of each musical feature due to the length of recorded EEG data. Tonal features include Mode and Key Clarity, which represent the strength of major of minor mode and the measure of tonal clarity, respectively. Rhythmic features include Fluctuation Centroid, Fluctuation Entropy, and Pulse Clarity. Fluctuation centroid is the geometric mean of the fluctuation spectrum representing the global repartition of rhythm periodicities within the range of 0–10 Hz. Fluctuation Entropy is the Shannon entropy of the fluctuation spectrum representing the global repartition of rhythm periodicities. Pulse Clarity is an estimate of clarity of the pulse.

C. Source Reconstruction

Source reconstruction procedure was performed with open-source Brainstorm software [42]. For forward modeling, we used the symmetric boundary element method (BEM) to compute the volume-conductor model with the MNI-ICBM152 template corresponding to a grid of 15000 cortical sources. For source modeling, minimum norm estimate (MNE) was applied with a measure of the current density map and constrained dipole orientations (normal to cortex). Then, the Desikan-Killiany anatomical atlas was used to parcellate the cortical surface into $C = 68$ regions, and the principal component analysis (PCA) method was performed to construct the time course for each brain region.

D. Dynamic Functional Connectivity

Many studies have reported that the communication of brain regions or neural populations depends on phase interactions for electrophysiological neuroimaging techniques, like EEG [43]. To avoid source leakage, the pairwise synchronization was estimated by PLI to map the whole-brain FC [44]. In this study, to assess the dFC across both time and frequency, we segmented the source-space data into $W = 500$ windows by the sliding window technique with a window length of 3 s and an overlap of 2 s according to the extraction framework of musical features. Then, we computed the time-frequency (TF) decomposition within each time window by the continuous wavelet transform with Morlet wavelets as basis function . We set the frequency bins as 0.5 Hz, and obtained $F = 59$ samples in frequency domain in the range of 1-30 Hz.

For the time window w, we can get the complex TF representation $P_w \in \mathbb{R}^{T_w \times F}$ from wavelet transform, where $T_w = 3fs$, and the time and frequency-dependent phase at time t_w and frequency f can be obtained by

$$\varphi(t_w, f) = \arctan \frac{imag(P_w(t_w, f))}{real(P_w(t_w, f))}, \tag{3}$$

where $imag()$ and $real()$ represent the imaginary part and the real part of a complex value, respectively. For brain regions i and j, PLI can be computed as

$$PLI_{i,j}(w, f) = \frac{1}{T_w} \left| \sum_{t_w=1}^{T_w} sign(\triangle\varphi_{i,j}(t_w, f)) \right|, \tag{4}$$

where $\triangle\varphi_{i,j}(t_w, f)) = \varphi_i(t_w, f) - \varphi_j(t_w, f)$ is the phase difference of brain regions i and j at time t_w and frequency f in time window w. Therefore, for each time window and each frequency point, we can form an adjacency matrix $\boldsymbol{A} \in \mathbb{R}^{C \times C}$, where C means the number of brain regions. Because of the symmetry of FC matrix, we took the upper triangle of $\boldsymbol{A}$ and vectorized it to $\boldsymbol{a} \in \mathbb{R}^{N \times 1}$, where $N = C(C-1)/2 = 2278$ represents the number of unique connections. Then, we can construct two adjacency tensors with the dimension of time $\times$ frequency $\times$ connectivity $\times$ subject, $\boldsymbol{\mathcal{X}}^{\mathrm{HC}} \in \mathbb{R}^{W \times F \times N \times S_{\mathrm{HC}}}$ ($500 \times 59 \times 2278 \times 19$) for the HC group and $\boldsymbol{\mathcal{X}}^{\mathrm{MDD}} \in \mathbb{R}^{W \times F \times N \times S_{\mathrm{MDD}}}$ ($500 \times 59 \times 2278 \times 20$) for the MDD group, where $S_{\mathrm{HC}} = 19$ and $S_{\mathrm{MDD}} = 20$ mean the number of subjects in the HC group and the MDD group, respectively.

E. The Application of Low-Rank Coupled Tensor Decomposition

Considering the high computation load, the nonnegativity of the tensors (constrained to [0,1] due to PLI index) and high correlations in spatial and spectral modes, we applied a low-rank DC-NTD model which was more flexible to add desired constraints.

1) Low-Rank Coupled Tensor Decomposition: With the constructed tensors $\boldsymbol{\mathcal{X}}^{\mathrm{HC}} \in \mathbb{R}^{W \times F \times N \times S_{\mathrm{HC}}}$ and $\boldsymbol{\mathcal{X}}^{\mathrm{MDD}} \in \mathbb{R}^{W \times F \times N \times S_{\mathrm{MDD}}}$, the corresponding CP decomposition can be represented as $\boldsymbol{\mathcal{X}}^{\mathrm{HC}} \simeq \sum_{r=1}^{R_{\mathrm{HC}}} \boldsymbol{u}_r^{(1)} \circ \boldsymbol{u}_r^{(2)} \circ \boldsymbol{u}_r^{(3)} \circ \boldsymbol{u}_r^{(4)} = [\![\boldsymbol{U}^{(1)}, \boldsymbol{U}^{(2)}, \boldsymbol{U}^{(3)}, \boldsymbol{U}^{(4)}]\!]$ and $\boldsymbol{\mathcal{X}}^{\mathrm{MDD}} \simeq \sum_{r=1}^{R_{\mathrm{MDD}}} \boldsymbol{v}_r^{(1)} \circ \boldsymbol{v}_r^{(2)} \circ \boldsymbol{v}_r^{(3)} \circ \boldsymbol{v}_r^{(4)} = [\![\boldsymbol{V}^{(1)}, \boldsymbol{V}^{(2)}, \boldsymbol{V}^{(3)}, \boldsymbol{V}^{(4)}]\!]$, where $\circ$ denotes the vector outer product. $\boldsymbol{u}_r^{(n)}$ and $\boldsymbol{v}_r^{(n)}$ denote the rth component of factor matrices $\boldsymbol{U}^{(n)}$ and $\boldsymbol{V}^{(n)}$, $n = 1, 2, 3, 4$, in the modes of time, frequency, connectivity and subject for two groups. R_{HC} and R_{MDD} are the ranks of $\boldsymbol{\mathcal{X}}^{\mathrm{HC}}$ and $\boldsymbol{\mathcal{X}}^{\mathrm{MDD}}$, respectively. Considering the nonnegativity of constructed tensors and the coupled constraints in spectral and adjacency modes, we formulate it as a double-coupled nonnegative tensor decomposition (DC-NTD) model, where $\boldsymbol{\mathcal{X}}^{\mathrm{HC}}$ and $\boldsymbol{\mathcal{X}}^{\mathrm{MDD}}$ can be jointly analyzed by minimizing the following objective function:

$$\begin{aligned} &\mathcal{J}(\boldsymbol{u}_r^{(n)}, \boldsymbol{v}_r^{(n)}) \\ &= \|\boldsymbol{\mathcal{X}}^{\mathrm{HC}} - \sum_{r=1}^{R_{\mathrm{HC}}} \boldsymbol{u}_r^{(1)} \circ \boldsymbol{u}_r^{(2)} \circ \boldsymbol{u}_r^{(3)} \circ \boldsymbol{u}_r^{(4)}\|_F^2 \\ &\quad + \|\boldsymbol{\mathcal{X}}^{\mathrm{MDD}} - \sum_{r=1}^{R_{\mathrm{MDD}}} \boldsymbol{v}_r^{(1)} \circ \boldsymbol{v}_r^{(2)} \circ \boldsymbol{v}_r^{(3)} \circ \boldsymbol{v}_r^{(4)}\|_F^2 \\ &\quad \text{s.t.}\, \boldsymbol{u}_r^{(2)} = \boldsymbol{v}_r^{(2)} (r \le L_f),\ \boldsymbol{u}_r^{(3)} = \boldsymbol{v}_r^{(3)} (r \le L_c). \end{aligned} \tag{5}$$

$\|\cdot\|_F$ denotes the Frobenius norm. L_f and L_c denote the number of components coupled in spectral and adjacency modes, and $L_{f,c} \le \min(R_{\mathrm{HC}}, R_{\mathrm{MDD}})$. The fast hierarchical

alternative least squares (FHALS), an accelerated version of the hierarchical alternative least squares (HALS) algorithm, has been effectively applied to a number of (coupled) tensor decomposition problems [25], [45], [46]. In this study, we apply the FHALS algorithm to optimize the DC-NTD problem in (5), and introduce the low-rank approximation to reduce computational complexity [47], [48].

Through the FHALS algorithm, the minimization problem in (5) can be converted into $\max(R_{\mathrm{HC}}, R_{\mathrm{MDD}})$ rank-1 subproblems, which can be solved sequentially and iteratively. We take the rth subproblem as an example:

$$\begin{aligned}\min \mathcal{J}_r = &\|\mathcal{Y}_r^{\mathrm{HC}} - \boldsymbol{u}_r^{(1)} \circ \boldsymbol{u}_r^{(2)} \circ \boldsymbol{u}_r^{(3)} \circ \boldsymbol{u}_r^{(4)}\|_F^2 \\ &+\|\mathcal{Y}_r^{\mathrm{MDD}} - \boldsymbol{v}_r^{(1)} \circ \boldsymbol{v}_r^{(2)} \circ \boldsymbol{v}_r^{(3)} \circ \boldsymbol{v}_r^{(4)}\|_F^2, \quad (6)\end{aligned}$$

where $\mathcal{Y}_r^{\mathrm{HC}} \doteq \mathcal{X}^{\mathrm{HC}} - \sum_{k\neq r}^{R_{\mathrm{HC}}} \boldsymbol{u}_k^{(1)} \circ \boldsymbol{u}_k^{(2)} \circ \boldsymbol{u}_k^{(3)} \circ \boldsymbol{u}_k^{(4)}$ and $\mathcal{Y}_r^{\mathrm{MDD}} \doteq \mathcal{X}^{\mathrm{MDD}} - \sum_{k\neq r}^{R_{\mathrm{MDD}}} \boldsymbol{v}_k^{(1)} \circ \boldsymbol{v}_k^{(2)} \circ \boldsymbol{v}_k^{(3)} \circ \boldsymbol{v}_k^{(4)}$. When calculating one of the variables, we need to fix the other variables and let the corresponding derivative be zero. For example, to determine $\boldsymbol{u}_r^{(n)}$, we let $\partial \mathcal{J}_r / \partial \boldsymbol{u}_r^{(n)}$ be zero, and then we can obtain the following solution:

$$\boldsymbol{u}_r^{(n)} = \boldsymbol{Y}_{r,(n)}^{\mathrm{HC}} \left[\boldsymbol{u}_r\right]^{\odot -n} / \left[\boldsymbol{u}_r{}^T \boldsymbol{u}_r\right]^{\circledast -n}, \quad (7)$$

where $\boldsymbol{Y}_{r,(n)}^{\mathrm{HC}}$ is the mode-n matricization of $\mathcal{Y}_r^{\mathrm{HC}}$. $\odot$ and $\circledast$ denote the Khatri-Rao product and Hadamard (element-wise) product. $\left[\boldsymbol{u}_r\right]^{\odot -n} = \boldsymbol{u}_r^{(4)} \odot \cdots \odot \boldsymbol{u}_r^{(n+1)} \odot \boldsymbol{u}_r^{(n-1)} \odot \cdots \odot \boldsymbol{u}_r^{(1)}$ and $\left[\boldsymbol{u}_r{}^T \boldsymbol{u}_r\right]^{\circledast -n} = \left([\boldsymbol{u}_r]^{\odot -n}\right)^T [\boldsymbol{u}_r]^{\odot -n}$. Taking $\boldsymbol{Y}_{r,(n)}^{\mathrm{HC}} = \boldsymbol{X}_{(n)}^{\mathrm{HC}} - \boldsymbol{U}^{(n)}[\boldsymbol{U}^{\odot -n}]^T + \boldsymbol{u}_r^{(n)}[\boldsymbol{u}_r^{\odot -n}]^T$ into (7), we can get

$$\boldsymbol{u}_r^{(n)} = \boldsymbol{u}_r^{(n)} + \left[\boldsymbol{X}_{(n)}^{\mathrm{HC}} \boldsymbol{u}_r^{\odot -n} - \boldsymbol{U}^{(n)} \boldsymbol{\Gamma}_r^{(n)}\right] / \boldsymbol{\Gamma}_{(r,r)}^{(n)}, \quad (8)$$

where $\boldsymbol{X}_{(n)}^{\mathrm{HC}}$ is the mode-n matricization of $\mathcal{X}^{\mathrm{HC}}$ and $\boldsymbol{\Gamma}^{(n)} = \left[\boldsymbol{U}^T \boldsymbol{U}\right]^{\circledast -n}$. Suppose that the rank-$\tilde{R}_{\mathrm{HC}}$ approximation of $\mathcal{X}^{\mathrm{HC}}$ obtained by unconstrained tensor factorization is expressed as $[\![\tilde{\boldsymbol{U}}^{(1)}, \tilde{\boldsymbol{U}}^{(2)}, \tilde{\boldsymbol{U}}^{(3)}, \tilde{\boldsymbol{U}}^{(4)}]\!]$, $\tilde{R}_{\mathrm{HC}} \leq R_{\mathrm{HC}}$, thus the mode-$n$ unfolding of $\mathcal{X}^{\mathrm{HC}}$ can be written as $\boldsymbol{X}_{(n)}^{\mathrm{HC}} = \tilde{\boldsymbol{U}}^{(n)} \left[\tilde{\boldsymbol{U}}^{\odot -n}\right]^T$. Therefore, the learning rule of $\boldsymbol{u}_r^{(n)}$ can be reformulated as follows:

$$\boldsymbol{u}_r^{(n)} = \boldsymbol{u}_r^{(n)} + \left[\tilde{\boldsymbol{U}}^{(n)} \tilde{\boldsymbol{\Gamma}}_r^{(n)} - \boldsymbol{U}^{(n)} \boldsymbol{\Gamma}_r^{(n)}\right] / \boldsymbol{\Gamma}_{(r,r)}, \quad (9)$$

where $\tilde{\boldsymbol{\Gamma}}^{(n)} = [\tilde{\boldsymbol{U}}^T \boldsymbol{U}]^{\circledast -n}$. Analogously, we can obtain the learning rule of $\boldsymbol{v}_r^{(n)}$ as follows:

$$\boldsymbol{v}_r^{(n)} = \boldsymbol{v}_r^{(n)} + \left[\tilde{\boldsymbol{V}}^{(n)} \tilde{\boldsymbol{\Lambda}}_r^{(n)} - \boldsymbol{V}^{(n)} \boldsymbol{\Lambda}_r^{(n)}\right] / \boldsymbol{\Lambda}_{(r,r)}^{(n)}, \quad (10)$$

where $\boldsymbol{\Lambda}^{(n)} = \left[\boldsymbol{V}^T \boldsymbol{V}\right]^{\circledast -n}$ and $\tilde{\boldsymbol{\Lambda}}^{(n)} = [\tilde{\boldsymbol{V}}^T \boldsymbol{V}]^{\circledast -n}$. The rank-$\tilde{R}_{\mathrm{MDD}}$ approximation of $\mathcal{X}^{\mathrm{MDD}}$ is expressed as $[\![\tilde{\boldsymbol{V}}^{(1)}, \tilde{\boldsymbol{V}}^{(2)}, \tilde{\boldsymbol{V}}^{(3)}, \tilde{\boldsymbol{V}}^{(4)}]\!]$, $\tilde{R}_{\mathrm{MDD}} \leq R_{\mathrm{MDD}}$. Specially, if $r \leq L_f$, $\boldsymbol{u}_r^{(2)} = \boldsymbol{v}_r^{(2)}$ and if $r \leq L_c$, $\boldsymbol{u}_r^{(3)} = \boldsymbol{v}_r^{(3)}$, thus their solutions should be calculated as:

$$\begin{aligned}\boldsymbol{u}_r^{(2)} &= \boldsymbol{v}_r^{(2)} \\ &= \boldsymbol{u}_r^{(2)} + \left[\tilde{\boldsymbol{U}}^{(2)} \tilde{\boldsymbol{\Gamma}}_r^{(2)} - \boldsymbol{U}^{(2)} \boldsymbol{\Gamma}_r^{(2)} + \tilde{\boldsymbol{V}}^{(2)} \tilde{\boldsymbol{\Lambda}}_r^{(2)} - \boldsymbol{V}^{(2)} \boldsymbol{\Lambda}_r^{(2)}\right] \\ &\quad / \left[\boldsymbol{\Gamma}_{(r,r)}^{(2)} + \boldsymbol{\Lambda}_{(r,r)}^{(2)}\right], \quad (11)\end{aligned}$$

and

$$\begin{aligned}\boldsymbol{u}_r^{(3)} &= \boldsymbol{v}_r^{(3)} \\ &= \boldsymbol{u}_r^{(3)} + \left[\tilde{\boldsymbol{U}}^{(3)} \tilde{\boldsymbol{\Gamma}}_r^{(3)} - \boldsymbol{U}^{(3)} \boldsymbol{\Gamma}_r^{(3)} + \tilde{\boldsymbol{V}}^{(3)} \tilde{\boldsymbol{\Lambda}}_r^{(3)} - \boldsymbol{V}^{(3)} \boldsymbol{\Lambda}_r^{(3)}\right] \\ &\quad / \left[\boldsymbol{\Gamma}_{(r,r)}^{(3)} + \boldsymbol{\Lambda}_{(r,r)}^{(3)}\right], \quad (12)\end{aligned}$$

In order to obtain the nonnegative components, a simple "half-rectifying" nonlinear projection is applied. We update $\boldsymbol{u}_r^{(n)}$ and $\boldsymbol{v}_r^{(n)}$ successively in each subproblem, and the $\max(R_{\mathrm{HC}}, R_{\mathrm{MDD}})$ subproblems are optimized alternatively one after another until convergence. In this study, we adopt alternating least squares (ALS, [49]) algorithm to perform low-rank approximation. The FHALS-based DC-NTD algorithm is summarized in **Algorithm** 1.

Algorithm 1 DC-NTD-FHALS Algorithm

Input: $\mathcal{X}^{\mathrm{HC}}$, $\mathcal{X}^{\mathrm{MDD}}$, L_f, L_c, R_{HC}, R_{MDD}, $\tilde{R}_{\mathrm{HC}}$, $\tilde{R}_{\mathrm{MDD}}$
Initialization: $\boldsymbol{U}^{(n)}$, $\boldsymbol{V}^{(n)}$, $n = 1, 2, 3, 4$
Calculate $\tilde{\boldsymbol{U}}^{(n)}$, $\tilde{\boldsymbol{V}}^{(n)}$, $n = 1, 2, 3, 4$ via unconstrained ALS
while *unconvergence* **do**
  for $n = 1, 2, \cdots, 4$ **do**
    for $r = 1, 2, \cdots max(R_{HC}, R_{MDD})$ **do**
      Update $\boldsymbol{u}_r^{(n)}$, $\boldsymbol{u}_r^{(n)}$ via (9), (10), (11) and (12)
    end
  end
end
Output: $\boldsymbol{U}^{(n)}$, $\boldsymbol{V}^{(n)}$, $n = 1, 2, 3, 4$

2) Selection of Components: In this section, we will describe how to determine the number of totally extracted components R_{HC} and R_{MDD}, which refers to the hidden information in low-dimensional space for each block data, and the number of coupled components L_f and L_c, which reveal the common features between two-block data. For the selection of R_{HC} and R_{MDD}, we performed PCA on the matricization data $\mathcal{X}_{(3)} \in \mathbb{R}^{F \times WNS}$ unfolded along frequency mode for each block data, and kept the number of components with 95% explained variance. The selection of the number of coupled components is a key issue for the conduction of the DC-NTD-FHALS algorithm and the explanation of results, and it always becomes an open issue depending on practical applications. In this study, we performed the fourth-order CP tensor decomposition based on the FHALS algorithm on two-block data separately, and calculated the correlation maps of extracted components between two-block data in spectral and adjacency modes, respectively. According to the correlation maps, we will select the number of highly correlated (coupled) components. The detailed implication procedure will be described in the results section.

F. Identification of Music-Induced Hyperconnectivity and Hypoconnectivity Networks

After the conduction of the low-rank DC-NTD-FHALS algorithm, we need to identify the music-induced oscillatory

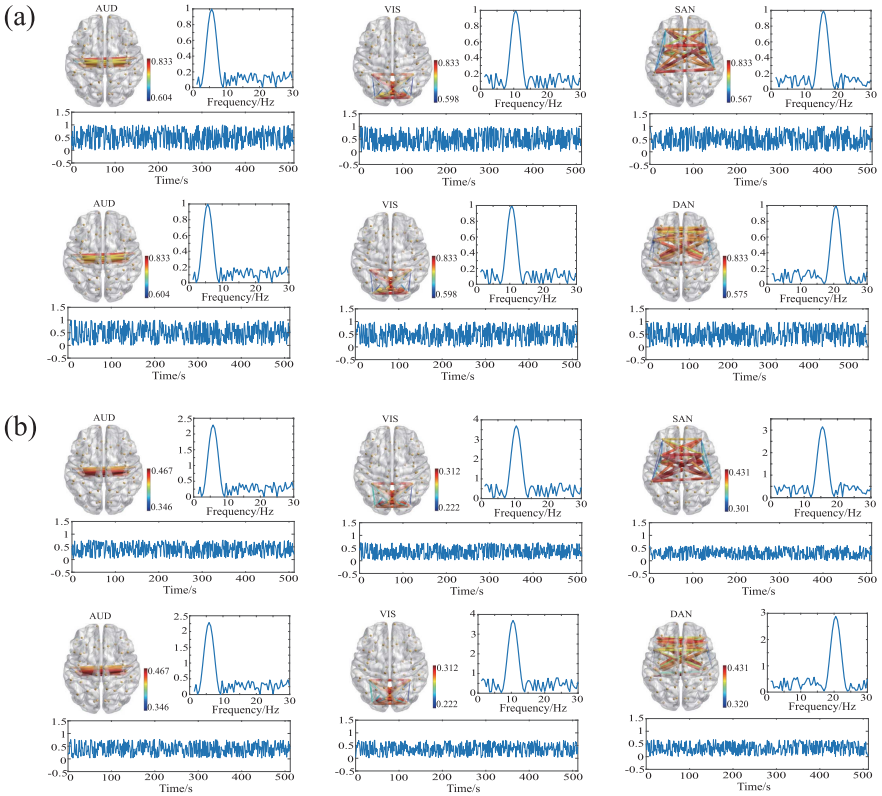

Fig. 2. Simulation illustration. (a) Three spatio-temporal-spectral patterns were simulated for two groups, and the first two patterns were identical in adjacency and spectral modes. (b) The reconstructed spatio-temporal-spectral patterns.

networks that are abnormal involved in the MDD group. We conducted a correlation analysis approach between temporal factors and five musical features with Pearson correlation based on the permutation test method. To ensure the statistical significance of the correlation and consider the problem of multiple comparison, the Monte Carlo method and permutation test were applied to compute a significant threshold of correlation for each musical feature [21]–[23], [25]. For the time course of each musical feature, we kept the real part and replaced the imaginary part with random uniformly distributed phases, and performed Pearson correlation with the time courses of the extracted temporal components. Then, we repeated this procedure 100000 times, and obtained the threshold for each musical feature at a significant level of $p_{corrected} < 0.05$.

The coupled spectral and adjacency components are common features between CON and MDD groups, and the remaining components are individual features of each group. The oscillatory networks among common features that are involved in music perception in the HC group but not in the MDD group are identified as hypoconnectivity networks, and the oscillatory networks among individual features that are involved in music perception in the MDD group are identified as hyperconnectivity.

III. Results

A. Results of Simulated Data

We implemented the low-rank DC-NTD-FHALS algorithm on the synthetic data, and we set $SNR = 15$, $L_f = L_c = 2$, and $R_{\text{HC}} = R_{\text{MDD}} = 3$. The extracted temporal, spectral and adjacency factors were shown in Figure 2(b). We ran 10 times of the low-rank DC-NTD-FHALS algorithm, and we obtained stable decomposition results with an averaged tensor fit of 0.864 and an averaged running time of 113.27 seconds.

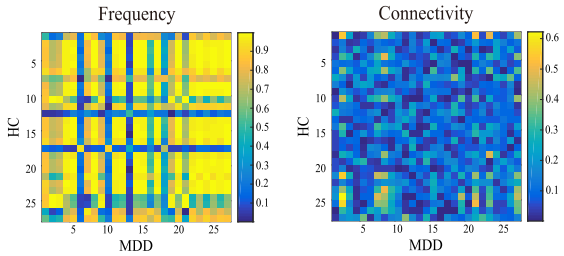

Fig. 3. Correlation analysis of the spectral factor and the adjacency factor extracted from the 4-D tensor decomposition for each block data.

B. Results of EEG Data

Through PCA analysis on the unfolded data along the spectral mode for two-block data, we extracted $R_{HC} = R_{MDD} = 27$ components for both HC group and MDD group. Then we performed the fourth-order CP tensor decomposition on each block data, and computed the correlation maps of spectral and adjacency factors between two groups, as shown in Figure 3. According to the correlation maps, we set the number of coupled components in the spectral mode $L_f = 25$ and the number of coupled components in the adjacency mode $L_c = 7$. We ran 20 times of the low-rank DC-NTF-FHALS algorithm,

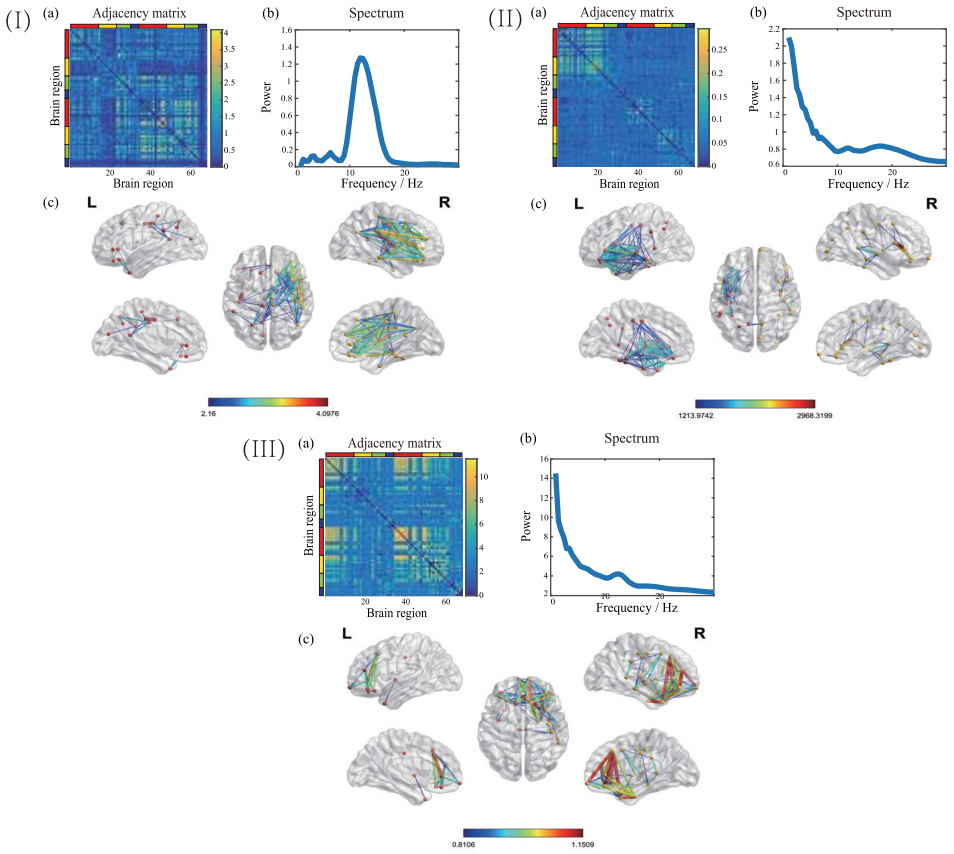

Fig. 4. Three oscillatory hyperconnectivity networks. (a) Adjacency matrix representation of the network. The 68 brain regions are ordered from the left hemisphere to the right hemisphere. Within each hemisphere, the brain regions are arranged in the order of frontal lobe, temporal lobe, parietal lobe, and occipital lobe, as indicated in red, yellow, green, and blue color, respectively. Within each lobe, the brain regions are ordered according to their y-location from anterior regions to posterior regions. (b) The spectral component of the network. (c) Cortical space representation of the network in Lateral, medial and dorsal view. The networks I, II, and III are related to the musical features of Fluctuation Centroid, Fluctuation Centroid, and Key Clarity, respectively.

and the averaged running time was 12616 seconds. The running time was 63819 seconds by one implementation of the DC-NTF-FHALS algorithm without the low-rank approximation, which indicated that the low-rank approximation could greatly reduce the computational load.

After applying the low-rank DC-NTF-FHALS algorithm and correlation analysis with musical features, we summarized the results of 20 times of implementation and obtained three oscillatory hyperconnectivity networks, as shown in Figure 4, and three oscillatory hypoconnectivity networks, as shown in Figure 5. For hyperconnectivity networks, Figure 4I shows a right hemisphere dominated network modulated by oscillations of alpha and beta (10-16 Hz) bands and the musical feature of Fluctuation Centroid. The strong connections of this network connect the core regions of DMN, including medial prefrontal cortex (mPFC), precuneus cortex, and posterior cingulate cortex (PCC). Figure 4II indicates a left auditory-related network modulated by delta oscillations and the Fluctuation Centroid feature. An aberrant delta-specific prefrontal network is identified, which is related to the musical feature of Key Clarity, as shown in Figure 4III. For hypoconnectivity networks, Figure 5I and Figure 5II exhibit fronto-parietal networks which are mainly related to attention control. The fronto-parietal networks are modulated by oscillations of 8-14 Hz and 10-19 Hz and musical features of Mode and Fluctuation Entropy, respectively. Figure 5III shows a low-frequency (delta oscillations) modulated prefrontal network which is significantly related to the musical feature of Mode, and this network is implicated in complex cognitive functions.

IV. Discussion

As far as we know, this study is the first attempt to investigate the aberrant dFC across temporal evolution and spectral modulation in MDD during music listening based on a coupled tensor decomposition approach. This study proposed a comprehensive framework to extract the FC networks characterized by spatio-temporal-spectral modes of covariation. We summarized three overactive oscillatory networks and three underactive oscillatory networks according to the analysis of musical modulations.

MDD is characterized with imbalanced communications among large-scale functional networks, including hyperconnectivity and hypoconnectivity within specific brain networks or between distinct brain networks during resting-state, see a meta-analysis in study [6]. In our study, we also found hyperconnectivity and hypoconnectivity functional networks in naturalistic music perception. We identified a right hemisphere dominated hyperconnectivity network which involved the essential regions of DMN, including mPFC, PCC and precuneus cortex, as shown in Figure 4I.

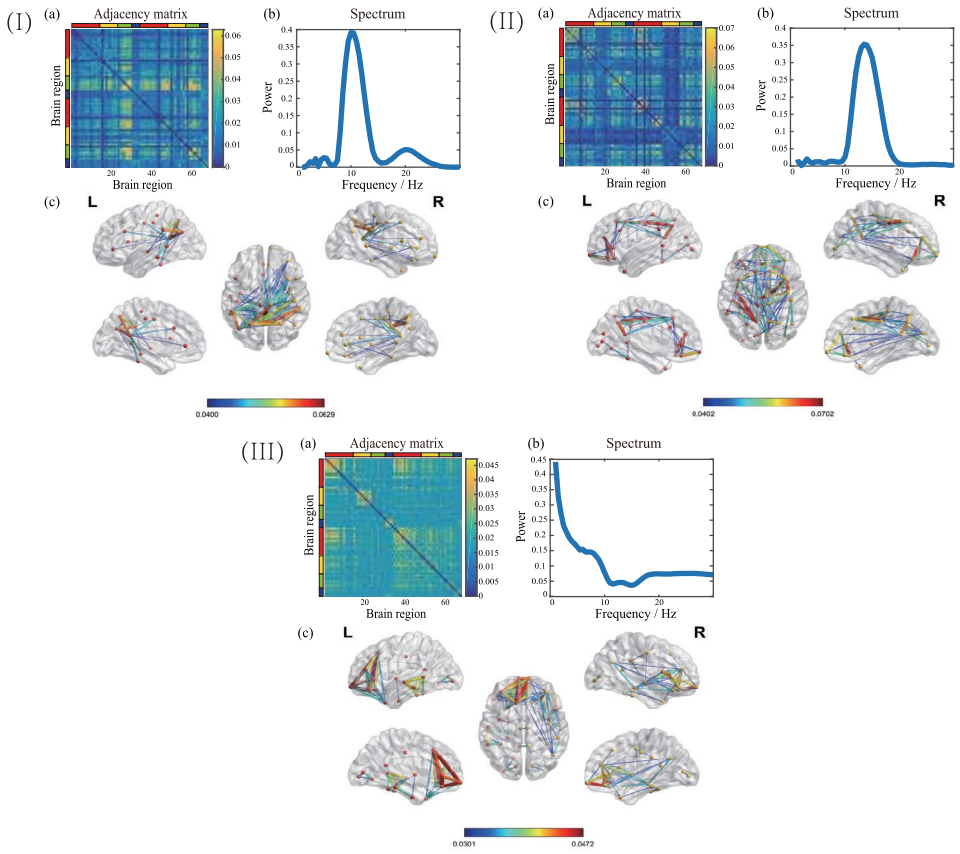

Fig. 5. Three oscillatory hypoconnectivity networks. (a) Adjacency matrix representation of the network. The 68 brain regions are ordered from left hemisphere to right hemisphere. Within each hemisphere, the brain regions are arranged in the order of frontal lobe, temporal lobe, parietal lobe, and occipital lobe, as indicated in red, yellow, green, and blue color, respectively. Within each lobe, the brain regions are ordered according to their y-location from anterior regions to posterior regions. (b) The spectral component of the network. (c) Cortical space representation of the network in Lateral, medial and dorsal view. The networks I, II, and III are related to the musical features of Mode, Fluctuation Entropy, and Fluctuation Entropy, respectively.

The hyperconnectivity in DMN are often considered as reflecting rumination, where MDD patients perseverate on negative, self-referential thoughts [50], [51]. Many researches have reported the hyperconnectivity within DMN in MDD, which supports that within-DMN hyperconnectivity is related to enhanced the positive connectivity in MDD [6], [51]. Figure 4II shows a delta band-modulated and left auditory-related network, which is activated by a rhythmic feature of Fluctuation Centroid. The delta band was demonstrated to have a substantial influence on the identification of natural speech fragments in a MEG study [52], and the decoding of rhythmic features was found to be significantly correlated with the auditory cortex during music perception [21], [53]. The abnormal delta band-modulated and left auditory-related network identified in our study might indicate that MDD patients were less involved in music perception. We identified two delta band modulated prefrontal networks, both of which were related to tonal features, Key Clarity and Mode, as shown in Figure 4III and Figure 5III. However, the prefrontal network in Figure 4III was hyperactive and right hemisphere lateralized, and the prefrontal network in Figure 5III was hypoactive and left hemisphere lateralized. The prefrontal cortex has been implicated in planning complex cognitive behavior, decision making and working memory. There are numerous lines of evidence demonstrating that prefrontal cortex is dysregulated in depression, and both increased and decreased functional connections in the prefrontal network may lead to the failure of inhibitory control in depression [54]–[57]. Those two prefrontal networks also have abnormal connections with temporal poles, which may indicate the dysfunction in semantic integration during music listening [58], [59]. Our findings are well supported by those literatures that the dysconnectivity in the prefrontal network can influence the high-order cognitive functions and information integration during music perception in MDD. Figure 5I and Figure 5II indicate hypoconnectivity fronto-parietal networks modulated by different oscillations and musical features. The abnormal development of the fronto-parietal network is a common feature across many psychiatric disorders with the deficit in cognitive control. Previous studies have demonstrated that MDD is characterized by hypoconnectivity within the frontoparietal network, which is involved in the top-down modulation of attention and emotion [6], [19], [60].

In our study, the key issue of applying coupled tensor decomposition is the selection of the number of all the extracted components and the number of coupled components. There are several methods for the selection of the number of extracted components in tensor/matrix decomposition, such as

PCA, the difference of fit (DIFFIT), model order selection, and so on [31]. In our study, due to that the spectral mode retains the minimum samples compared with temporal and adjacency modes, we applied PCA on the unfolded data along the spectral mode to determine the number of extracted components. We believe this unfolding format can help to approach the true underlying low-dimensional space. However, the selection of the number of coupled components and the coupled modes mainly relys on the data characteristics. Refer to our previous study, we use a correlation analysis in the spectral and adjacency modes in our study [25].

The scales of the reconstructed spatial, temporal and spectral factors are different from those in the synthetic data, see Figure 2. The scale indeterminacy will not change the topology of networks, the evolution of time courses and the modulation of oscillations. However, the addition of the constraints on scales will increase the model complexity and computational cost. In the present study, we only consider the group differences between HC and MDD groups by extracting the common features and individual features. Subject differences are omitted and covered in the residuals of the coupled tensor decomposition, and we assume that the extracted components are shared by all the subjects within each group. The problem of subject differences may bring more challenges, but it is also a crucial and realistic issue, especially in clinical applications.

We clarify two important limitations in this study. First, we do not have the anatomical images from the individual participant, and we use the MNI-ICBM152 template in forwarding modeling. Using the same anatomical MRI will influence the accuracy of source reconstruction. Second, the results have limited explanations due to the music type we selected. Further studies should investigate different music types, and we also need to consider the music preferences of participants.

V. Conclusion

In this study, we investigated the oscillatory hyperconnectivity and hypoconnectivity networks elicited by musical stimuli in MDD. Considering the high-dimensional structure of the datasets and group differences between HC and MDD groups, a comprehensive framework was proposed based on coupled tensor decomposition, and six abnormal connectivity networks with spatio-temporal-spectral modes of covariation were identified in MDD during music listening. Our findings are well supported and verified by previous literatures. Our research may serve as a signature of the brain's functional topography characterizing MDD, and provide novel biomarkers for the clinical diagnosis and treatment in MDD. The spectral profiles and spatial networks are usually characterized with sparsity, and the sparse regularization will be considered in the coupled tensor decomposition model in the future work. The neural correlates and dynamic neural processing of musical emotions have not been well studied, and the future work will also focus on the selection of control stimuli.

Acknowledgment

This study is to memorize Prof. Tapani Ristaniemi for his great help to the authors Fengyu Cong, Wenya Liu, and Xiulin Wang.

References

[1] I. H. Gotlib and J. Joormann, "Cognition and depression: Current status and future directions," *Annu. Rev. Clin. Psychol.*, vol. 6, no. 1, pp. 285–312, Mar. 2010.
[2] P. C. Mulders, P. F. van Eijndhoven, A. H. Schene, C. F. Beckmann, and I. Tendolkar, "Resting-state functional connectivity in major depressive disorder: A review," *Neurosci. Biobehav. Rev.*, vol. 56, pp. 330–344, Sep. 2015.
[3] G. Li *et al.*, "Large-scale dynamic causal modeling of major depressive disorder based on resting-state functional magnetic resonance imaging," *Hum. Brain Mapping*, vol. 41, no. 4, pp. 865–881, 2020.
[4] Y. I. Sheline, J. L. Price, Z. Yan, and M. A. Mintun, "Resting-state functional MRI in depression unmasks increased connectivity between networks via the dorsal nexus," *Proc. Nat. Acad. Sci. USA*, vol. 107, no. 24, pp. 11020–11025, 2010.
[5] M. Demirtaş *et al.*, "Dynamic functional connectivity reveals altered variability in functional connectivity among patients with major depressive disorder," *Hum. Brain Mapping*, vol. 37, no. 8, pp. 2918–2930, Aug. 2016.
[6] R. H. Kaiser, J. R. Andrews-Hanna, T. D. Wager, and D. A. Pizzagalli, "Large-scale network dysfunction in major depressive disorder: A meta-analysis of resting-state functional connectivity," *JAMA Psychiatry*, vol. 72, no. 6, pp. 603–611, 2015.
[7] A. Maratos, C. Gold, X. Wang, and M. Crawford, "Music therapy for depression," *Cochrane Database Systematic Rev.*, vol. 1, 2008.
[8] R. Ramirez, M. Palencia-Lefler, S. Giraldo, and Z. Vamvakousis, "Musical neurofeedback for treating depression in elderly people," *Frontiers Neurosci.*, vol. 9, p. 354, Oct. 2015.
[9] A. Dharmadhikari *et al.*, "Frontal theta asymmetry as a biomarker of depression," *East Asian Arch. Psychiatry*, vol. 28, no. 1, p. 17, 2018.
[10] W. Liu *et al.*, "Functional connectivity of major depression disorder using ongoing EEG during music perception," *Clin. Neurophysiol.*, vol. 131, no. 10, pp. 2413–2422, Oct. 2020.
[11] C. Chang and G. H. Glover, "Time–frequency dynamics of resting-state brain connectivity measured with fMRI," *NeuroImage*, vol. 50, no. 1, pp. 81–98, 2010.
[12] E. A. Allen, E. Damaraju, S. M. Plis, E. B. Erhardt, T. Eichele, and V. D. Calhoun, "Tracking whole-brain connectivity dynamics in the resting state," *Cerebral Cortex*, vol. 24, no. 3, pp. 663–676, 2014.
[13] R. H. Kaiser *et al.*, "Dynamic resting-state functional connectivity in major depression," *Neuropsychopharmacology*, vol. 41, no. 7, pp. 1822–1830, 2016.
[14] J. Wang *et al.*, "Abnormal dynamic functional network connectivity in unmedicated bipolar and major depressive disorders based on the triple-network model," *Psychol. Med.*, vol. 50, no. 3, pp. 465–474, Feb. 2020.
[15] G. Buzsaki, *Rhythms of the Brain*. London, U.K.: Oxford Univ. Press, 2006.
[16] A. A. Fingelkurts and A. A. Fingelkurts, "Altered structure of dynamic electroencephalogram oscillatory pattern in major depression," *Biol. Psychiatry*, vol. 77, no. 12, pp. 1050–1060, Jun. 2015.
[17] Y. Yan *et al.*, "Human cortical networking by probabilistic and frequency-specific coupling," *NeuroImage*, vol. 207, Feb. 2020, Art. no. 116363.
[18] L. E. Gascoyne *et al.*, "Motor-related oscillatory activity in schizophrenia according to phase of illness and clinical symptom severity," *NeuroImage, Clin.*, vol. 29, Jan. 2021, Art. no. 102524.
[19] A. E. Whitton, S. Deccy, M. L. Ironside, P. Kumar, M. Beltzer, and D. A. Pizzagalli, "Electroencephalography source functional connectivity reveals abnormal high-frequency communication among large-scale functional networks in depression," *Biol. Psychiatry, Cognit. Neurosci. Neuroimag.*, vol. 3, no. 1, pp. 50–58, Jan. 2018.
[20] A. A. Fingelkurts, A. A. Fingelkurts, H. Rytsälä, K. Suominen, E. Isometsä, and S. Kähkönen, "Impaired functional connectivity at EEG alpha and theta frequency bands in major depression," *Hum. Brain Mapping*, vol. 28, no. 3, pp. 247–261, 2007.
[21] V. Alluri, P. Toiviainen, I. P. Jääskeläinen, E. Glerean, M. Sams, and E. Brattico, "Large-scale brain networks emerge from dynamic processing of musical timbre, key and rhythm," *NeuroImage*, vol. 59, no. 4, pp. 3677–3689, 2012.
[22] F. Cong *et al.*, "Linking brain responses to naturalistic music through analysis of ongoing EEG and stimulus features," *IEEE Trans. Multimedia*, vol. 15, no. 5, pp. 1060–1069, Aug. 2013.
[23] Y. Zhu, J. Liu, K. Mathiak, T. Ristaniemi, and F. Cong, "Deriving electrophysiological brain network connectivity via tensor component analysis during freely listening to music," *IEEE Trans. Neural Syst. Rehabil. Eng.*, vol. 28, no. 2, pp. 409–418, Feb. 2020.

[24] Y. Zhu *et al.*, "Exploring frequency-dependent brain networks from ongoing eeg using spatial ICA during music listening," *Brain Topography*, vol. 33, no. 3, pp. 289–302, 2020.

[25] X. Wang, W. Liu, P. Toiviainen, T. Ristaniemi, and F. Cong, "Group analysis of ongoing EEG data based on fast double-coupled nonnegative tensor decomposition," *J. Neurosci. Methods*, vol. 330, Jan. 2020, Art. no. 108502.

[26] N. Leonardi *et al.*, "Principal components of functional connectivity: A new approach to study dynamic brain connectivity during rest," *Neuroimage*, vol. 83, pp. 937–950, Dec. 2013.

[27] G. C. O'Neill *et al.*, "Measurement of dynamic task related functional networks using MEG," *NeuroImage*, vol. 146, pp. 667–678, Feb. 2017.

[28] C. Chatzichristos, E. Kofidis, L. De Lathauwer, S. Theodoridis, and S. Van Huffel, "Early soft and flexible fusion of EEG and fMRI via tensor decompositions," 2020, *arXiv:2005.07134*. [Online]. Available: http://arxiv.org/abs/2005.07134

[29] A. Cichocki, "Tensor decompositions: A new concept in brain data analysis?" 2013, *arXiv:1305.0395*. [Online]. Available: http://arxiv.org/abs/1305.0395

[30] T. G. Kolda and B. W. Bader, "Tensor decompositions and applications," *SIAM Rev.*, vol. 51, no. 3, pp. 455–500, 2009.

[31] F. Cong, Q.-H. Lin, L.-D. Kuang, X.-F. Gong, P. Astikainen, and T. Ristaniemi, "Tensor decomposition of EEG signals: A brief review," *J. Neurosci. Methods*, vol. 248, pp. 59–69, Jun. 2015.

[32] D. Wang, Y. Zhu, T. Ristaniemi, and F. Cong, "Extracting multi-mode ERP features using fifth-order nonnegative tensor decomposition," *J. Neurosci. Methods*, vol. 308, pp. 240–247, Oct. 2018.

[33] F. Miwakeichi, E. Martínez-Montes, P. A. Valdés-Sosa, N. Nishiyama, H. Mizuhara, and Y. Yamaguchi, "Decomposing EEG data into space–time–frequency components using parallel factor analysis," *NeuroImage*, vol. 22, no. 3, pp. 1035–1045, 2004.

[34] M. Mørup, L. K. Hansen, C. S. Herrmann, J. Parnas, and S. M. Arnfred, "Parallel factor analysis as an exploratory tool for wavelet transformed event-related EEG," *NeuroImage*, vol. 29, no. 3, pp. 938–947, 2006.

[35] Y. Zhu *et al.*, "Discovering dynamic task-modulated functional networks with specific spectral modes using MEG," *NeuroImage*, vol. 218, Sep. 2020, Art. no. 116924.

[36] G. Zhou *et al.*, "Linked component analysis from matrices to high-order tensors: Applications to biomedical data," *Proc. IEEE*, vol. 104, no. 2, pp. 310–331, Feb. 2016.

[37] Y. Jonmohamadi, S. Muthukumaraswamy, J. Chen, J. Roberts, R. Crawford, and A. Pandey, "Extraction of common task features in EEG-fMRI data using coupled tensor-tensor decomposition," *Brain Topography*, vol. 33, no. 5, pp. 636–650, Sep. 2020.

[38] B. Rivet, M. Duda, A. Guerin-Dugue, C. Jutten, and P. Comon, "Multimodal approach to estimate the ocular movements during EEG recordings: A coupled tensor factorization method," in *Proc. 37th Annu. Int. Conf. IEEE Eng. Med. Biol. Soc. (EMBC)*, Aug. 2015, pp. 6983–6986.

[39] A. Kabbara, W. EL Falou, M. Khalil, F. Wendling, and M. Hassan, "The dynamic functional core network of the human brain at rest," *Sci. Rep.*, vol. 7, no. 1, pp. 1–16, Dec. 2017.

[40] V. Alluri *et al.*, "From vivaldi to beatles and back: Predicting lateralized brain responses to music," *NeuroImage*, vol. 83, pp. 627–636, Dec. 2013.

[41] O. Lartillot and P. Toiviainen, "MIR in MATLAB (II): A toolbox for musical feature extraction form audio," in *Proc. 7th Int. Conf. Music Inf. Retr. (ISMIR)*, 2002, pp. 287–288.

[42] F. Tadel, S. Baillet, J. C. Mosher, D. Pantazis, and R. M. Leahy, "Brainstorm: A user-friendly application for MEG/EEG analysis," *Comput. Intell. Neurosci.*, vol. 2011, pp. 1–13, Oct. 2011.

[43] T. Womelsdorf *et al.*, "Modulation of neuronal interactions through neuronal synchronization," *Science*, vol. 316, no. 5831, pp. 1609–1612, 2007.

[44] C. J. Stam, G. Nolte, and A. Daffertshofer, "Phase lag index: Assessment of functional connectivity from multi channel EEG and MEG with diminished bias from common sources," *Hum. Brain Mapping*, vol. 28, no. 11, pp. 1178–1193, Nov. 2007.

[45] A. Cichocki, R. Zdunek, and S.-I. Amari, "Hierarchical ALS algorithms for nonnegative matrix and 3D tensor factorization," in *Proc. Int. Conf. Independ. Compon. Anal. Signal Separat.* Berlin, Germany: Springer, 2007, pp. 169–176.

[46] A. Cichocki and A.-H. Phan, "Fast local algorithms for large scale nonnegative matrix and tensor factorizations," *IEICE Trans. Fundam. Electron., Commun. Comput. Sci.*, vol. 92, no. 3, pp. 708–721, 2009.

[47] G. Zhou, A. Cichocki, and S. Xie, "Fast nonnegative matrix/tensor factorization based on low-rank approximation," *IEEE Trans. Signal Process.*, vol. 60, no. 6, pp. 2928–2940, Jun. 2012.

[48] X. Wang, "Coupled nonnegative matrix/tensor factorization in brain imaging data," JYU dissertations, Dept. Inf. Technol., Univ. Jyväskylä, Jyväskylä, Finland, 2020.

[49] A. Cichocki, R. Zdunek, A. H. Phan, and S.-I. Amari, *Nonnegative Matrix and Tensor Factorizations: Applications to Exploratory Multi-Way Data Analysis and Blind Source Separation*. Hoboken, NJ, USA: Wiley, 2009.

[50] Y. I. Sheline *et al.*, "The default mode network and self-referential processes in depression," *Proc. Nat. Acad. Sci. USA*, vol. 106, no. 6, pp. 1942–1947, 2009.

[51] M. G. Berman, S. Peltier, D. E. Nee, E. Kross, P. J. Deldin, and J. Jonides, "Depression, rumination and the default network," *Social Cognit. Affect. Neurosci.*, vol. 6, no. 5, pp. 548–555, Oct. 2011.

[52] M. Koskinen, J. Viinikanoja, M. Kurimo, A. Klami, S. Kaski, and R. Hari, "Identifying fragments of natural speech from the listener's MEG signals," *Hum. Brain Mapping*, vol. 34, no. 6, pp. 1477–1489, Jun. 2013.

[53] P. Toiviainen, V. Alluri, E. Brattico, M. Wallentin, and P. Vuust, "Capturing the musical brain with lasso: Dynamic decoding of musical features from fMRI data," *NeuroImage*, vol. 88, pp. 170–180, Mar. 2014.

[54] B. D. Hare and R. S. Duman, "Prefrontal cortex circuits in depression and anxiety: Contribution of discrete neuronal populations and target regions," *Mol. Psychiatry*, vol. 25, no. 1, pp. 2742–2758, 2020.

[55] M. S. George, T. A. Ketter, and R. M. Post, "Prefrontal cortex dysfunction in clinical depression," *Depression*, vol. 2, no. 2, pp. 59–72, 1994.

[56] S. F. Taylor and I. Liberzon, "Neural correlates of emotion regulation in psychopathology," *Trends Cognit. Sci.*, vol. 11, no. 10, pp. 413–418, Oct. 2007.

[57] M. R. Bennett, "The prefrontal–limbic network in depression: A core pathology of synapse regression," *Prog. Neurobiol.*, vol. 93, no. 4, pp. 457–467, Apr. 2011.

[58] M. P. van den Heuvel, R. C. W. Mandl, C. J. Stam, R. S. Kahn, and H. E. H. Pol, "Aberrant frontal and temporal complex network structure in schizophrenia: A graph theoretical analysis," *J. Neurosci.*, vol. 30, no. 47, pp. 15915–15926, Nov. 2010.

[59] K. Tsapkini, C. E. Frangakis, and A. E. Hillis, "The function of the left anterior temporal pole: Evidence from acute stroke and infarct volume," *Brain*, vol. 134, no. 10, pp. 3094–3105, Oct. 2011.

[60] J. L. Vincent, I. Kahn, A. Z. Snyder, M. E. Raichle, and R. L. Buckner, "Evidence for a frontoparietal control system revealed by intrinsic functional connectivity," *J. Neurophysiol.*, vol. 100, no. 6, pp. 3328–3342, Dec. 2008.